Conformational Locking upon Cooperative Assembly of Notch Transcription Complexes

Sung Hee Choi,[1] Thomas E. Wales,[2] Yunsun Nam,[3,4] Daniel J. O'Donovan,[3,4] Piotr Sliz,[3,4] John R. Engen,[2] and Stephen C. Blacklow[1,3,5,*]

[1]Department of Cancer Biology, Dana-Farber Cancer Institute, Boston, MA 02115, USA
[2]Department of Chemistry and Chemical Biology, Barnett Institute of Chemical & Biological Analysis, Northeastern University, Boston, MA 02115, USA
[3]Department of Biological Chemistry and Molecular Pharmacology, Harvard Medical School, Boston, MA 02115, USA
[4]Laboratory of Molecular Medicine, Children's Hospital, Boston, MA 02115, USA
[5]Department of Pathology, Brigham and Women's Hospital, Boston, MA 02115, USA
*Correspondence: sblacklow@rics.bwh.harvard.edu
DOI 10.1016/j.str.2011.12.011

SUMMARY

The Notch intracellular domain (NICD) forms a transcriptional activation complex with the DNA-binding factor CSL and a transcriptional co-activator of the Mastermind family (MAML). The "RAM" region of NICD recruits Notch to CSL, facilitating the binding of MAML at the interface between the ankyrin (ANK) repeat domain of NICD and CSL. Here, we report the X-ray structure of a human MAML1/RAM/ANK/CSL/DNA complex, and probe changes in component dynamics upon stepwise assembly of a MAML1/NICD/CSL complex using HX-MS. Association of CSL with NICD exerts remarkably little effect on the exchange kinetics of the ANK domain, whereas MAML1 binding greatly retards the exchange kinetics of ANK repeats 2-3. These exchange patterns identify critical features contributing to the cooperative assembly of Notch transcription complexes (NTCs), highlight the importance of MAML recruitment in rigidifying the ANK domain and stabilizing its interface with CSL, and rationalize the requirement for MAML1 in driving cooperative dimerization of NTCs on paired-site DNA.

INTRODUCTION

Notch receptors are type I transmembrane proteins that communicate essential signals in response to transmembrane ligands expressed on neighboring cells. These signals control a wide range of cellular events both during development and in normal tissue homeostasis (Artavanis-Tsakonas et al., 1999; Bray, 2006; Kopan and Ilagan, 2009). Dysregulated Notch signaling is also associated with developmental anomalies and cancer, most notably in tumors of the immune system and of the squamous epithelial lineage (Agrawal et al., 2011; Klinakis et al., 2011; Puente et al., 2011; Stransky et al., 2011; Weng et al., 2004).

In mammals, there are four Notch receptors and five canonical Notch ligands (DLL1, DLL3, DLL4, JAG1, and JAG2). Canonical Notch signals are initiated when ligand binding triggers shedding of the Notch ectodomain by a metalloprotease of the a disintegrin and metalloprotease (ADAM) family (Brou et al., 2000; Mumm et al., 2000). Metalloprotease cleavage generates a truncated Notch molecule that is a substrate for the gamma secretase multiprotein enzyme complex, which liberates the intracellular portion of Notch (NICD) from the cytoplasmic side of the plasma membrane. NICD then enters the nucleus, where it assembles into a nuclear transcriptional activation complex that induces the expression of Notch target genes (Kopan and Ilagan, 2009; Kovall and Blacklow, 2010).

The core components of Notch nuclear complexes (Figure 1) include NICD, a DNA-binding factor called CSL (gene name RBPJ), and a coactivator protein of the Mastermind family (MAML). In the case of human Notch1, NICD contains a RAM (RBP-J-associated molecule) sequence, an ankyrin (ANK)-repeat domain with seven repeats, a transactivation region (TAD), and a C-terminal PEST sequence (Figure 1A). CSL consists of three core domains, an N-terminal Rel-homology domain (NTD), a beta-trefoil domain (BTD), and a C-terminal Rel homology domain (CTD). MAML proteins such as Mastermind-like-1 (MAML1) comprise a short N-terminal region, required for Notch transcription complex (NTC) assembly, followed by lower-complexity sequences reported to recruit other coactivator proteins such as p300 (Fryer et al., 2002; Wallberg et al., 2002) and components of the mediator complex such as Cyclin c/CDK8 (Fryer et al., 2004).

Biochemical and structural studies of NTCs from mammals and worms have led to a working model for complex assembly (Figure 1B). These studies have shown that the RAM module of Notch engages the BTD of CSL and contributes most of the affinity for CSL binding, whereas the ANK repeat domain, which appears to have a weak intrinsic affinity for CSL, associates with the NTD and CTD domains of CSL to create a binding groove for the N-terminal segment of MAML proteins (Bertagna et al., 2008; Del Bianco et al., 2008; Friedmann et al., 2008; Lubman et al., 2007; Nam et al., 2006; Wilson and Kovall, 2006). These protein-protein interactions occur in the absence of DNA, and the association of CSL with DNA appears to exert little influence on the affinities of individual protein components for one another (Kovall and Blacklow, 2010).

Despite these advances, a number of questions regarding complex assembly remain unsettled. First, there are no structures of mammalian NTCs that include the RAM region, and as
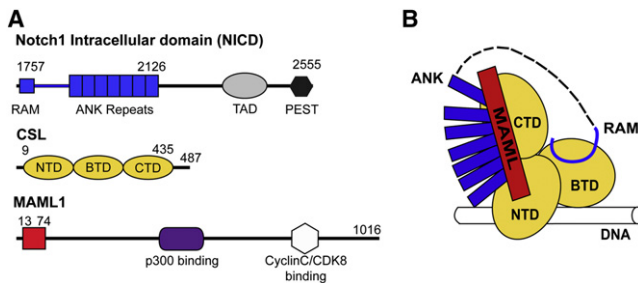
Figure 1. Components of Nuclear Notch Transcription Complexes
(A) Top: domain organization of the NICD, denoting the RAM region, ANK repeats, a transcriptional activation domain (TAD), and the PEST sequence implicated in receptor degradation. Middle: domain organization of CSL, denoting the NTD, BTD, and CTD. Bottom: organization of MAML1, identifying the N-terminal polypeptide required for assembly of NTCs (red), a region implicated in binding p300 (purple), and the C-terminal portion implicated in recruitment of Cyclin C:cdk8 complexes (white). Domains of the proteins utilized in these studies are colored blue (Notch1), yellow (CSL), and red (MAML1).
(B) Schematic of the core components of the human NTC, illustrating the Notch ANK and RAM regions (blue), the MAML1 helix (red), and the three domains of CSL (yellow) on DNA (cylinder).

a result the precise mode of RAM binding to CSL has not yet been determined for these complexes. Second, it is not clear whether RAM-mediated recruitment of mammalian NICD to CSL leads to stable docking of the ANK domain onto the CTD and NTD of CSL, or whether this step merely increases the effective concentration of the ANK domain for its binding site by constraining it to remain nearby (Bertagna et al., 2008). Whereas FRET assays have shown that transfer from a donor site on the ANK domain to an acceptor on CSL-bound DNA occurs upon association of RAMANK proteins with CSL (Del Bianco et al., 2008), calorimetry studies indicate that the binding enthalpy associated with association of RAMANK and CSL is not distinguishable from binding of RAM to CSL, suggesting that the interface between the ANK domain and CSL is either incompletely formed or in dynamic equilibrium with an open conformation in the absence of MAML1 (VanderWielen et al., 2011). Last, cooperative assembly of dimeric Notch transcription complexes requires the presence of MAML1, even though the only visible contacts between the individual NTCs in the crystal structure of the dimeric complex lie in the second and third ANK repeats of the Notch ANK domain (Arnett et al., 2010; Nam et al., 2007), raising the question of how this cooperativity is orchestrated biochemically.

Here, we have combined X-ray crystallography and hydrogen exchange mass spectrometry (HX-MS) to clarify several key facets of mammalian NTC assembly. The X-ray structure of the RAM/ANK/MAML1/CSL/DNA complex defines the interface between RAM and CSL in a mammalian Notch1 complex for the first time, to our knowledge, and shows that a conformational change in the human CSL protein need not occur to accommodate binding of the RAM peptide (Barrick and Kopan, 2006). The HX-MS studies identify critical features contributing to the cooperative assembly of NTCs, and highlight the importance of MAML recruitment in rigidifying the ANK domain and stabilizing its interface with CSL. The HX-MS data also rationalize the known requirement for MAML1 in enabling the cooperative

dimerization of NTCs on paired-site DNA and suggest that MAML1 recruitment disfavors competitive binding of putative transcriptional repressors, securing the expression of Notch responsive genes.

RESULTS

X-ray Structure of a RAM/ANK/MAML1/CSL/DNA Complex
The structure of a Notch1 RAM/ANK/MAML1/CSL/DNA complex was determined to 3.85 Å resolution by molecular replacement, using the structure of the Notch1 ANK/MAML1/CSL/DNA complex as a search model (Table S1 and Figure S1 available online). The components used to solve the structure of the complex included residues 9–435 of CSL (RBPJ isoform 6 in the current NCBI database), residues 13–74 of human MAML1, the ANK domain of human Notch1 (comprising residues M1872–G2126), a 19-residue RAM peptide from human Notch1 (KRRRQHGQLWFPEGFKVSE), and a blunt-ended 18-base-pair DNA duplex from the proximal promoter of the human HES-1 gene. The structure was refined as part of a pilot project for a newly created deformable elastic network (DEN) portal (http://sbgrid.org; O'Donovan et al., 2012; Schröder et al., 2007, 2010).

The binding of RAM preserves the overall architecture of the NTC, and occurs without substantial movement in any of the other components: CSL, ANK, MAML1, or bound DNA (Figure 2A). The RAM peptide binds to a groove normally occupied by a beta-hairpin in proteins with a β-trefoil fold but missing from the BTD in CSL (Friedmann et al., 2008; Kovall and Hendrickson, 2004; Wilson and Kovall, 2006). Residues conserved between C. elegans and humans occupy analogous positions in human and worm complexes, but the path of the RAM peptide differs after the highly conserved WΦP sequence (where Φ represents a hydrophobic residue), which fills a large hydrophobic pocket on the surface of the BTD (Figure 2B). The differences most likely arise as a result of differences between the human and worm proteins in the residues C-terminal to the WΦP sequence. Whereas in the worm protein the residues following this sequence are PME (Figure 2B), the analogous three residues in the human protein are EGF.

HX-MS Global Exchange Profiles
In order to investigate the basis for cooperative assembly of the human Notch1 NTC, we utilized the technique of HX-MS (Johnson and Walsh, 1994; Katta and Chait, 1991; Zhang and Smith, 1993). Hydrogen exchange, pioneered by Linderstrom-Lang, Englander, and others (Englander and Mayne, 1992; Hvidt and Linderstrøm-Lang, 1954), is ideally suited to probe protein dynamics and conformational transitions when structures of the complex and/or its components are available as reference states (Wales and Engen, 2006), and when the formation of the complex buries a large amount of surface area, as is true for NTCs (Table S2). Here, HX-MS was utilized to report on the changes in protein dynamics that occur in response to assembly of the ternary RAMANK/CSL/MAML1 complex from its three individual protein components.

First, we determined the effect of complex formation on the global hydrogen exchange patterns for each individual protein
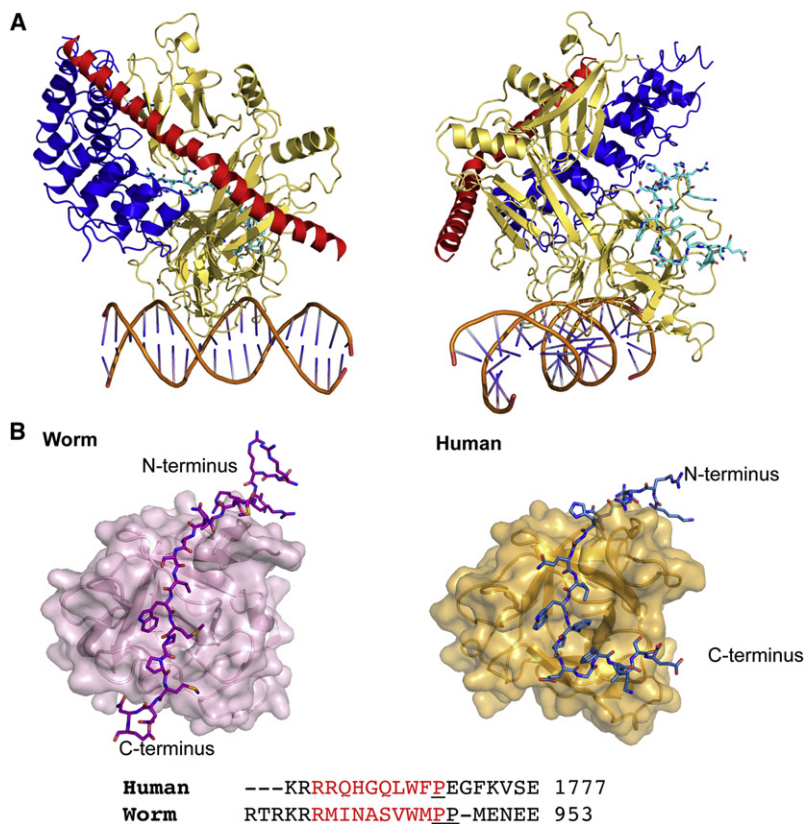
Figure 2. X-ray Crystal Structure of a Human NTC Core Containing MAML1, RAM, ANK, CSL, and Cognate DNA

(A) The human NTC structure showing the ANK repeats (blue), the CSL protein (yellow), the MAML1 polypeptide (red), DNA (orange), and the RAM polypeptide (cyan).

(B) Comparison of the human RAM-CSL interface (right) with that seen in the X-ray structure of the worm NTC (left; PDB ID code 2FO1), with the RAM peptides in stick format and the BTD shown as a transparent surface over cartoon representation. An alignment of the RAM residues observed in the two structures is shown below the structures. Residues in red occupy analogous positions in the two complexes.

Data in this figure are supported by Figure S1 and Table S1.

component (Figure 3). For the RAMANK protein, binding of CSL exerts a detectable but modest effect. Strikingly, further addition of MAML1 has a substantial additional effect that starts at the 10 s time point and persists over the entire time course of the experiment (Figure 3A). For CSL, the binding of RAMANK shows a consistent increase in protection from exchange throughout the time course; however, further addition of MAML1 does not have a large additional effect (Figure 3B). Finally, the isolated MAML1 polypeptide undergoes maximal exchange by the first time point (within 10 s), and becomes protected against exchange only upon formation of a ternary protein complex with both CSL and RAMANK (Figures 3C and 3D).

HX-MS Analysis at the Peptide Level

In order to map the specific structural elements of each protein that become protected from exchange upon complex assembly, we monitored the pattern of deuterium uptake in peptides generated by pepsin digestion after quenching the exchange reaction, analyzing the amount of deuterium in each peptide by MS. Peptide data sets from different complex states contained unique as well as common peptides found in all samples. Both matched and unique peptides were analyzed to evaluate dynamics of individual components or complexes as a function of time, whereas matched, common peptides were used for direct comparison between complex states (presented as plots and difference maps). Matched peptides cover 42% of CSL, 75% of RAMANK, and 81% of the MAML1 polypeptide (Figure S2). Though the peptide coverage of CSL is lower due to difficulty identifying identical NTD peptides for all samples, the

overall peptide coverage (matching and unique peptides) is adequate for comparative analysis, especially given that the NTC is an ~100 kDa complex (the primary data are presented in Table S3 and Figure S3).

Protection Pattern of MAML1

For the MAML1 polypeptide, exchange is retarded upon complexation for residues between 21 and 66. Peptides in the N-terminus, in contrast, did not show any difference in exchange between the protein free and the protein in complex, and peptides in the C terminus also showed minimal differences at the earliest exchange time points (Figures 4 and S3A). A peptide spanning residues 38–51 (EARYEAVSPERLEL), located in the middle of the MAML1 polypeptide, exhibited particularly strong protection against exchange, indicating that this region is highly stabilized upon docking of MAML1 to the CSL-RAMANK complex. The observed length of the protected region is consistent with previous truncation studies analyzing complex formation in electrophoretic mobility-shift assays, which showed that deletion of 10 residues from either the N or the C terminus of the MAML1 polypeptide spanning residues 13–74 prevents efficient complex formation (Weng et al., 2003). It may be that exchange in the central region of the MAML1 polypeptide is most retarded because unfolding in the middle of the helix might depend on propagation of unfolding from one end or the other but otherwise fail to occur locally.

ANK Repeats 4–6 Constitute a Stable Core of the Notch Subunit of the Complex

Upon formation of complexes with CSL and MAML1, the ANK domain of Notch1 establishes an extensive interface with both the N- and C-terminal domains of CSL (NTD and CTD) and with MAML1 (Figure 5A), whereas the RAM region only contains a short peptide segment that interacts solely with the BTD of CSL (Figure 5B). In the isolated RAMANK polypeptide, the region including RAM and the linker leading to ANK are substantially deuterated at the initial (10 s) time point, and do not exhibit further exchange at later times (Figures 5C and S3B), indicating that this region remains unstructured in isolation. On the other hand, the different ANK repeats of the ANK domain exhibit
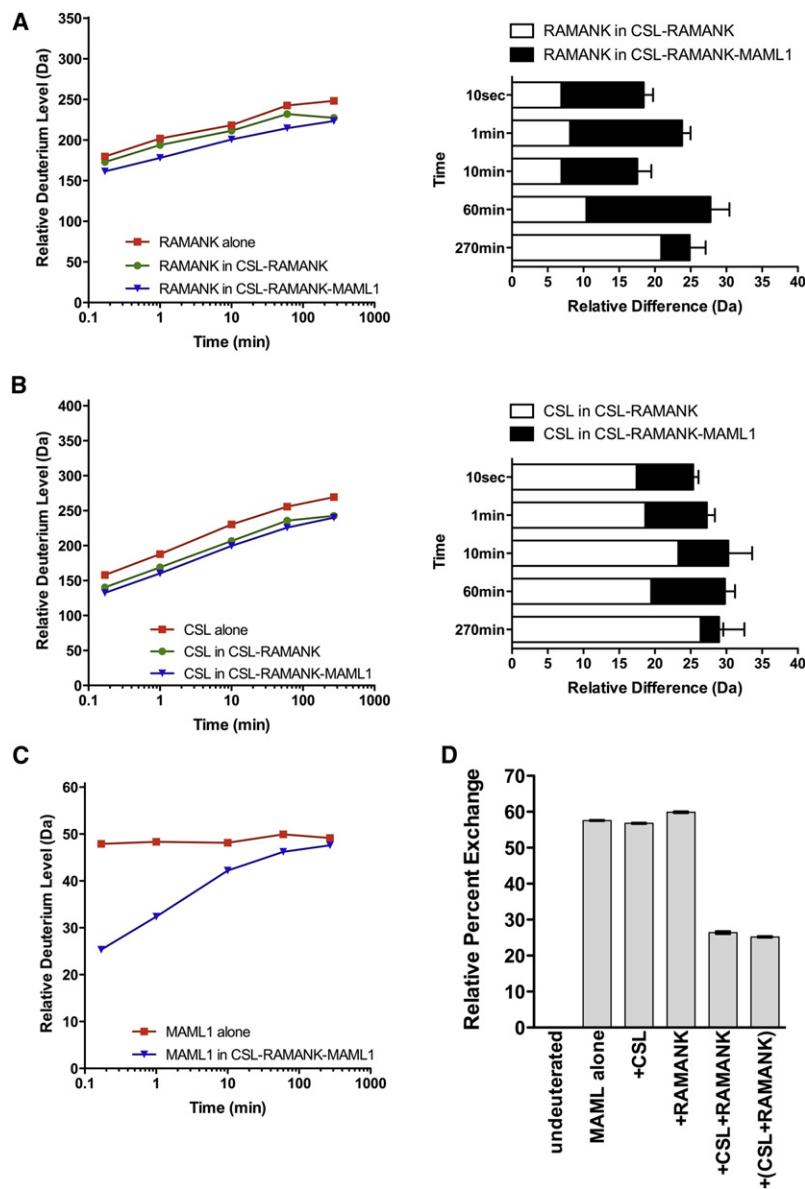
Figure 3. Global Hydrogen Exchange Profiles

(A–C) Time course of exchange, comparing deuteration of RAMANK (A), CSL (B), and MAML1 (C) as isolated proteins with that of RAMANK-CSL (A and B) and RAMANK-CSL-MAML1 (A–C) complexes. The relative difference in deuteration upon formation of RAMANK-CSL and RAMANK-CSL-MAML1 complexes, compared to isolated RAMANK (A) and CSL (B) proteins, is also plotted at right. (D) Percent exchange at the 10 s time point for various combinations of MAML1 with RAMANK and CSL. Error bars represent standard deviations from three or more replicates. Error bars for the deuteration data shown in A–C are frequently smaller than the peaks themselves. Data in this figure are supported by Figures S2 and S3 and Tables S2 and S3.

affinity for CSL, the RAM region shows substantial protection from exchange at early time points in the CSL-Notch complex, differences consistent with the X-ray structure of the complex with RAM bound (Figure 2). The exchange data also support the conclusion that the polypeptide segment connecting the RAM region to the ANK domain remains highly mobile upon formation of a complex with CSL (Figure S3B).

Though the exchange kinetics for the second and third ANK repeats are detectably slowed in the CSL-Notch complex, the most dramatic alteration in the exchange pattern of the ANK repeats takes place upon subsequent association of MAML1 with CSL-Notch complexes. When MAML1 binds to form the ternary complex, the deuterium uptake of peptides from ANK repeats 2 and 3 is greatly retarded when compared to that of CSL-Notch binary complexes (Figures 5E–5G).

Protection Pattern of CSL and Its Perturbation upon Formation of Complexes

In the absence of Notch or MAML1, the BTD of CSL undergoes slower exchange with solvent than do the NTD and CTD, which are more dynamic in isolation (Figure S5). The $\beta3$-$\beta4$ loop of the NTD ["NTD loop" (Figure 6A)], which adopts distinct conformations in various mammalian and *C. elegans* crystallographic complexes (Friedmann et al., 2008), is rapidly deuterated (Figure 6D, left), indicating that the human NTD loop is flexible in the absence of DNA and unlikely to adopt a preferred conformation in solution prior to complex assembly. These findings highlight and reinforce distinctions between mammalian and worm proteins suggested by previous crystallographic studies of CSL-DNA complexes, in which the NTD loop was less well ordered in the murine complex, as judged by its associated electron density (Friedmann et al., 2008). It also remains possible that association of CSL with DNA may affect the exchange behavior of the NTD loop and other NTD regions, since the NTD makes critical sequence-specific contacts with the DNA.

Upon binding of RAMANK to CSL, the rate of deuterium uptake is significantly retarded in the BTD strands that comprise

varying degrees of protection in the uncomplexed state, revealing differences in intrinsic dynamics across the ANK domain (Figures 5D–5K and S4). Whereas the peptides from ANK repeats 4–6 are most protected from deuterium uptake (~10% exchange at the initial time point), peptides from the terminal repeats, 1 and 7, achieve maximal exchange at the initial time point, indicating that these repeats are highly flexible in solution. Peptides from ANK repeats 1–3 also undergo more rapid exchange than the repeat 4-6 "core" (Figures 5 and S4), consistent with the reported proteolytic lability of the three N-terminal repeats (Lubman et al., 2005).

Effect of Complex Formation on the Notch Protection Pattern

Upon binding to the CSL subunit of the complex, the largest difference in the protection pattern of the Notch RAMANK protein occurs in the RAM peptide (Figure 5C). As predicted from its high
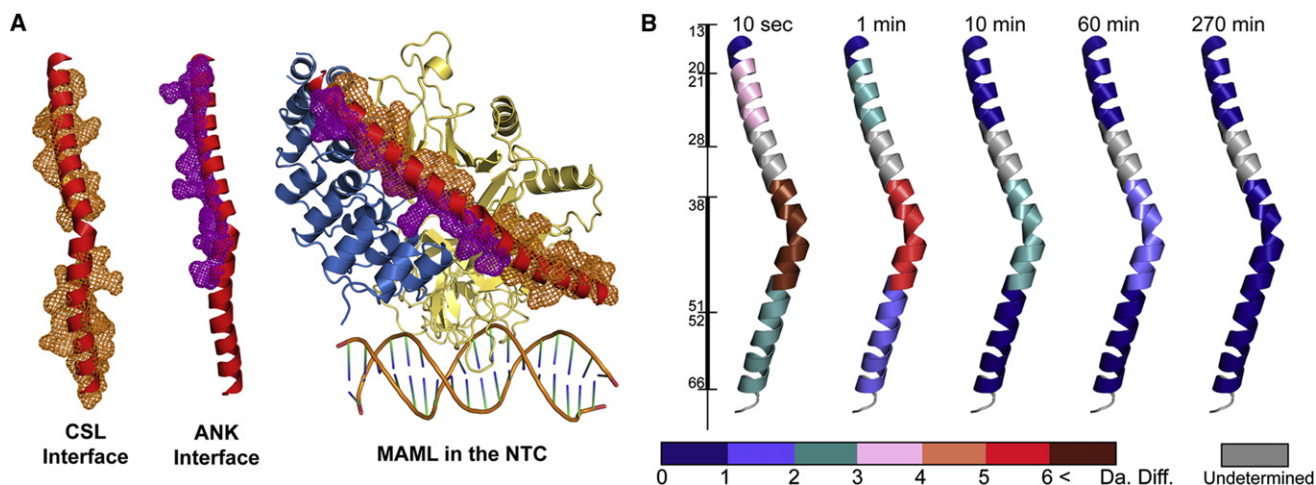
Figure 4. Local Exchange Profile of MAML1
(A) Cartoon representation of the MAML-1 polypeptide (red), with contacting residues from CSL (left) and ANK (center) illustrated in orange and purple mesh, respectively. The contact interface in the context of the full NTC is shown at right.
(B) Time course of exchange, comparing deuterium uptake of the MAML1 polypeptide in isolation with that observed in the CSL-RAMANK-MAML1 complex. The mass difference between MAML1 peptides (uncomplexed minus complexed) is mapped onto a cartoon representation of its conformation in the full complex, colored on a sliding scale from maroon (>6 Da) to dark blue (no difference). The black bar at the left denotes the sequence of the MAML1 polypeptide, with residue numbers and lines indicating the boundaries of specific peptides mapped onto the structure.
Data in this figure are supported by Figures S2 and S3A.

the RAM binding site in the new X-ray structure (Figures 2, 6B, and S6). On the other hand, the interface seen between ANK and CSL in the crystal structures of the ternary complexes (Figure 2; Nam et al., 2006) shows only minor reductions in deuterium uptake upon formation of CSL-RAMANK binary complexes (Figures 6D, 6E, and S5). Upon assembly of ternary complexes with both RAMANK and MAML1, the ANK-binding surface of CSL exhibits a decrease in deuterium uptake, which parallels the decreased uptake seen in ANK repeats 2 and 3 of the Notch1 polypeptide with full complex assembly. Accrual of MAML1 into the complex also retards deuterium uptake in the RAM-binding region of the BTD, perhaps by increasing the occupancy of RAM at this binding site by an avidity effect. Finally, ternary-complex formation retards exchange in the NTD-loop-containing peptide, consistent with the locking of this loop into its "down" conformation to accommodate MAML1 (Figures 6, S5, and S6).

DISCUSSION

The primary effectors of Notch signal transduction are nuclear complexes that contain CSL, Notch, and Mastermind proteins on target DNA. Previous structural studies and binding affinity measurements have shown that (1) the RAM region of Notch constitutes a high-affinity binding module for the BTD of CSL, and (2) the ANK domain of Notch together with the CTD and NTD of CSL create a composite binding site required to recruit Mastermind proteins into these complexes.

To our knowledge, we report the first structure of a mammalian NTC that contains the RAM peptide. The structure shows that RAM binds to CSL analogously in worms (Wilson and Kovall, 2006) and humans, but also points to subtle structural differences between complexes at sites of sequence divergence

C-terminal to the core binding motif (Figure 2). We have also examined the dynamics of individual NTC components and their changes upon complex formation in order to resolve several unanswered questions about the biochemistry of NTC assembly. The HX-MS studies uniquely complement the structural studies and affinity measurements, because they identify dynamic regions of the individual proteins and alterations in their flexibility upon protein-protein interaction, events that cannot be monitored crystallographically.

Regarding the minor structural differences between worm and human complexes, the divergence between worm and human RAM peptides is substantial, with residue identities only at the N-terminal KRR basic sequence and at the Trp and Pro of the LWFP sequence (Figure 2B). Alanine scanning studies from the Barrick laboratory using a mammalian consensus RAM sequence show that the LWFP sequence makes the greatest energetic contribution to peptide-BTD binding, and energetically significant contributions are also made by the N-terminal basic sequence. By contrast the EGF residues following the Pro of the conserved WFP make minor but detectable energetic contributions to BTD binding, and residues C-terminal to them have a negligible effect (Johnson et al., 2010). Intriguingly, EBNA2 has a WWPPIS sequence, and binding of an EBNA2 peptide is sensitive to the Q293L mutation of CSL (denoted Q307 previously, because CSL has several isoforms that differ at the N-terminal end), whereas the same mutation appears to enhance the affinity of CSL for the Notch RAM peptide. It may be that the differential effects of the mutation on RAM and EBNA2 binding reflect differences in the peptide exit path, with the EBNA2 peptide following the trajectory of the worm RAM peptide (which has a closely related WMPPME sequence), as opposed to the path of the Notch1 RAM peptide, which lacks the diproline motif and has a glycine residue that increases the
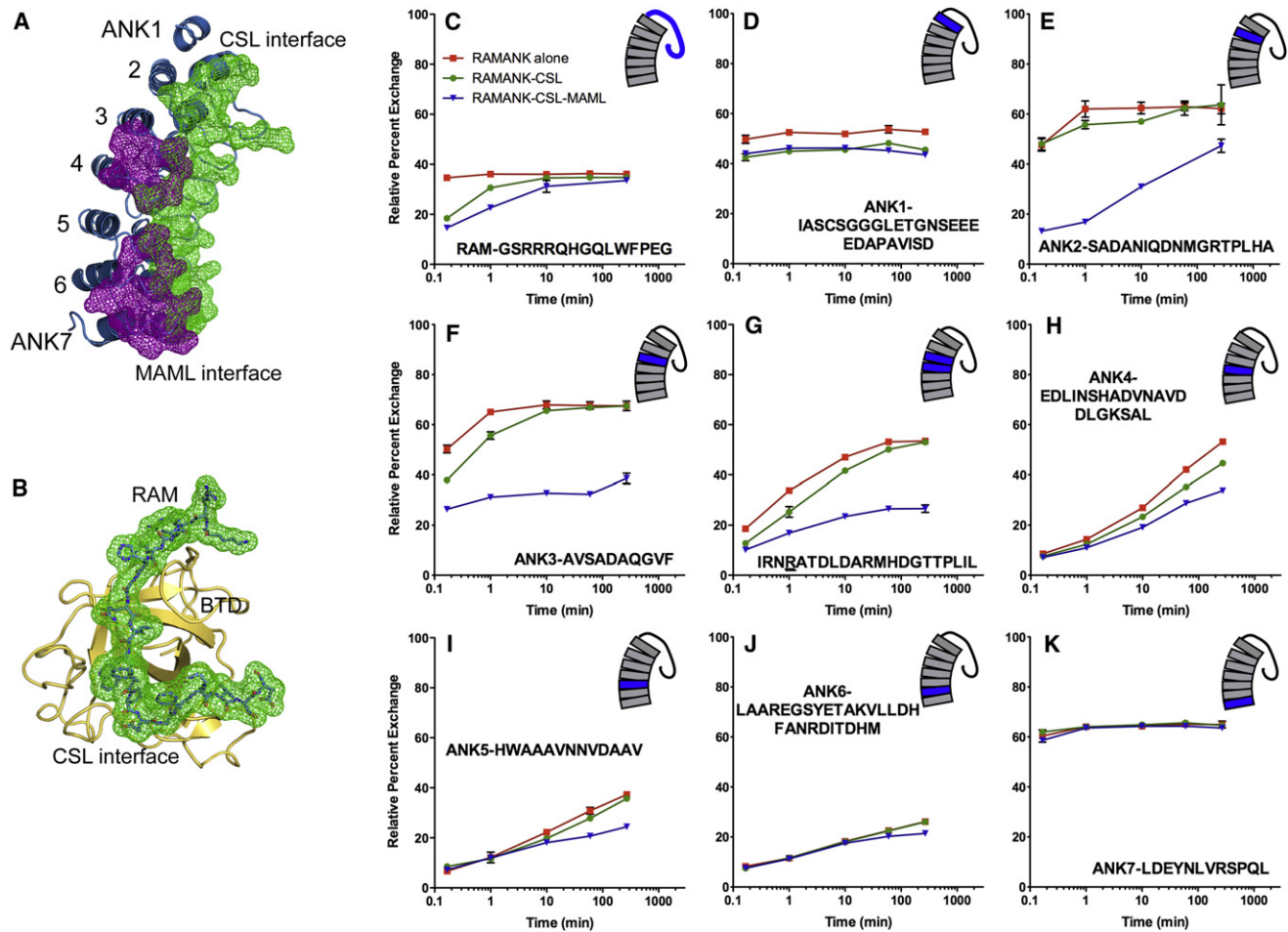
Figure 5. Local Exchange Profile of RAMANK

(A) Cartoon representation of the ANK domain of Notch1 (blue), with contacting residues from CSL and MAML1 illustrated in green and purple mesh, respectively.
(B) Interface of the RAM peptide (sticks and green mesh) with the BTD of CSL (yellow cartoon trace).
(C–K) Semilogarithmic plots showing the time course of exchange, comparing deuteration of peptides from RAMANK alone (red squares), RAMANK in complex with CSL (green circles), and RAMANK in complex with CSL and MAML1 (inverted blue triangles). The region of RAMANK represented by each peptide in C–K is indicated by the blue shading in the cartoon at the upper right corner of the plot. Error bars represent the range derived from analysis of duplicate measurements. Data in this figure are supported by Figures S2, S3B, S4, and S5.

conformational flexibility of the Notch1 peptide C-terminal to the WFP. It is also possible that the observed mode of binding for the Notch1 peptide may also have been influenced by the use of an isolated RAM peptide (as opposed to RAM covalently connected to the ANK domain by its natural sequence, as was true in the worm complexes), and that the minor conformational differences C-terminal to the WΦP reflect two possible binding modes with little energetic difference between them, revealed by the species differences and the different approaches to crystallization of complexes containing RAM. As the sequence of human Notch4 has both a diproline motif and a glycine residue following the second proline, it would be interesting to determine what the conformation of the Notch4 peptide is when bound.

The HX-MS studies of the isolated RAMANK polypeptide from human Notch1 identify a core region spanning ankyrin repeats 4–6 that is most greatly protected against hydrogen exchange in the native state. In contrast, studies of the ANK domain from *Drosophila* Notch identified a folding nucleus of repeats 3–5,

which overlaps with, but does not completely match, the core identified by HX-MS for the human protein (Bradley and Barrick, 2006; Mello and Barrick, 2004). There is 70% identity between the *Drosophila* Notch and human Notch1 ANK domains, but the greatest divergence among the internal repeats 2–6 is in repeat 5, where the identity is only 18/33 residues. If the HX-MS protection patterns indeed report only on ANK repeat stability in the native state, then we would attribute the differences between the *Drosophila* and human proteins to a C-terminally shifted folding nucleus that is a consequence of these or other amino acid sequence differences. However, it is possible that native-state hydrogen exchange (measured by HX-MS) and local stability measurements (extracted from analysis of global stabilities and folding/unfolding kinetics of Ala-Gly mutations introduced into each repeat) are assessing different facets of the folded domain.

The most striking changes in the kinetics of deuterium uptake observed upon complex formation take place in the second and
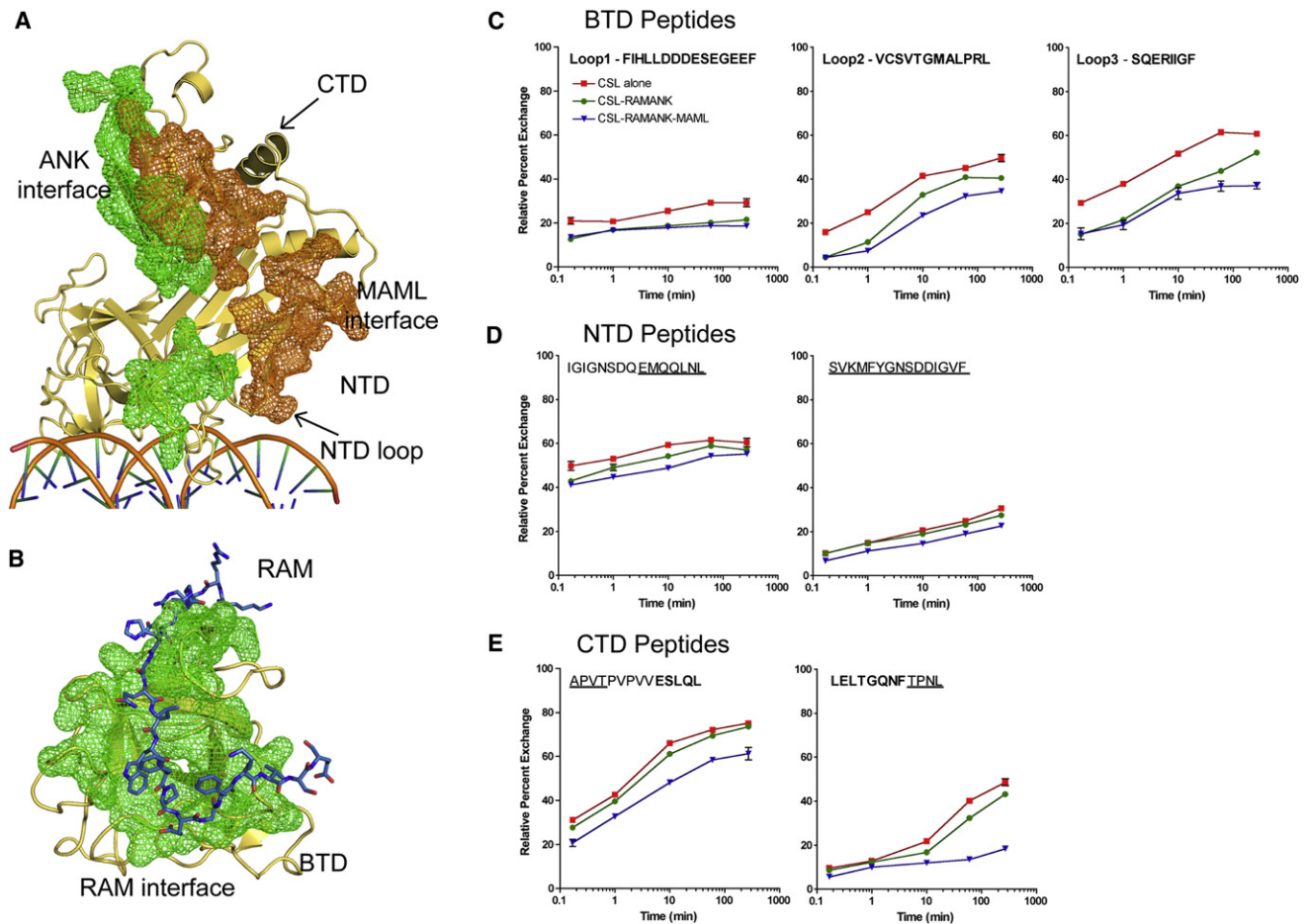
Figure 6. Local Exchange Profile of CSL

(A) Cartoon representation of CSL (yellow), with contacting residues from RAMANK and MAML1 illustrated in green and brown mesh, respectively.

(B) Cartoon representation of the BTD interacting with the RAM peptide (sticks). BTD residues contacting RAM are illustrated in green mesh.

(C–E) Semilogarithmic plots of exchange as a function of time for BTD peptides in the interface with RAM (C), NTD peptides in contact with MAML1 (D), and CTD peptides in the interface with ANK and MAML1 (E). Plots compare the extent of deuteration for CSL alone (red squares), CSL when complexed with RAMANK (green circles), and CSL in complex with RAMANK and MAML1 (inverted blue triangles). Underlined residues denote regions in contact with ANK, and bolded residues denote regions in contact with MAML-1. Error bars represent the range derived from analysis of duplicate measurements.

Data in this figure are supported by Figures S2, S3C, S5, and S6.

third repeats of the Notch ANK domain. The reduction in the rate of deuterium uptake seen upon binding of MAML1 to CSL-RAMANK complexes, which is much larger than the change in uptake seen upon association of RAMANK with CSL, indicates that the ANK-CSL interface is not fully engaged when MAML1 is not present (i.e., that the occupancy of ANK at its binding site on CSL is less than one in the absence of MAML1). Upon MAML1 binding, the ANK-CSL interface becomes locked shut, highly structured, and/or sealed away from effective penetration by solvent. Our working interpretation is that MAML1 binding retards exchange in ANK repeats 2 and 3 by stabilizing the folded conformation of these repeats when bound, because MAML1 binding does not greatly further retard exchange in ANK repeats 4-6, which are intrinsically more protected when unbound. These findings nicely complement previous reports that the affinity of ANK for CSL (>20 μM based on fluorescence measurements) is low by comparison to RAM (Del Bianco et al., 2008), and that the inclusion of ANK in the same polypeptide chain does

not enhance the binding enthalpy of RAM for CSL (VanderWielen et al., 2011).

The requirement that MAML1 be present to lock the ANK domain in place in the ternary complex also has implications for the assembly of dimeric NTCs. It is well established that cooperative assembly of dimeric NTCs occurs only when MAML1 has been added to Notch-CSL-DNA complexes (Arnett et al., 2010; Nam et al., 2007), yet the protein-protein interface seen in the X-ray structure of the NTC dimer only shows direct contacts between the ANK domain of one NTC and the ANK domain of the other (Arnett et al., 2010). Remarkably, the interactions between the two ANK domains also occur between residues in ANK repeat 2 (a salt bridge between K1946 and E1950) and residues in ANK repeat 3 [relying on interactions of R1983 and R1985 (Figure 5G)]. Thus, the requirement for MAML1 in cooperative assembly of dimeric NTCs likely results from its role in clamping the ANK domain in place when the ternary Notch-CSL-MAML complex is formed, which then permits the

ANK-ANK interactions to stabilize the dimeric NTCs on paired-site DNA.

Potential Use of HX-MS as a Probe of the Binding Interface for Other CSL-Associated Proteins

Recent studies investigating the interaction of the MINT core-pressor with CSL indicate that residues 2776–2833 of MINT bind to CSL with low nanomolar affinity (VanderWielen et al., 2011). This work implicates both the BTD and CTD of CSL in MINT binding, but the binding interface remains largely undetermined. In lieu of mapping the interface by exhaustive mutagenesis, which would be particularly challenging for a protein such as CSL because of its structural sensitivity to mutational changes, the HX-MS approach used here could be applied to CSL-MINT complexes to identify the binding interface rapidly and compare it to the Notch-CSL interface.

EXPERIMENTAL PROCEDURES

Protein Expression and Purification

The ANK domain (1872–2126), RAMANK domain (RAMANK: 1757–2126) of NICD, CSL (9–435), and MAML1 (13–74) were prepared as previously described (Nam et al., 2003, 2006). To prepare CSL-RAMANK and CSL-RAMANK-MAML1 complexes, the individual components were mixed in 1:3 and 1:3:10 molar ratios, respectively, and purified by size exclusion chromatography to eliminate uncomplexed subunits. Prior to hydrogen exchange, all proteins and their complexes were buffer-exchanged into size-exclusion buffer A (20 mM Tris, pH 8.5, 150 mM NaCl, and 5 mM DTT). For X-ray crystallographic studies, oligonucleotides from the human Hes-1 promoter (5′-GTTACTGTGGGAAAGAAA-3′ and 5′-TTTCTTTCCCA CAGTAAC-3′) were chemically synthesized (Integrated DNA Technologies) and purified by anion-exchange chromatography (BioscaleQ10, Bio-Rad) and annealed in TE buffer by slow cooling after heating at 95°C for 10 min. The RAM peptide (KRRRQHGQLWFPEGFKVSE) was chemically synthesized (Invitrogen) and purified over reverse-phase high performance liquid chromatography (HPLC).

X-ray Crystallography
Crystallization and Data Processing

To grow crystals of the multiprotein-DNA complex, we prepared Notch1 ANK/MAML1/CSL complexes as previously reported (Nam et al., 2006) and mixed them in 1:1.2:1.4 stoichiometry with the annealed DNA duplex and the RAM peptide of human Notch1. Crystals grew from hanging drops containing equal volumes of protein (5 mg/ml)/DNA solution and reservoir buffer (50 mM HEPES [pH 7.9], 6% PEG 3350, and 5% ethylene glycol). Crystals were cryoprotected by soaking in mother liquor supplemented with ethylene glycol (25%) for flash-freezing in liquid nitrogen. Data were collected at ID19, Structural Biology Center at Argonne National Laboratory. Data were indexed and scaled using HKL2000 (Otwinowski and Minor, 1997).

Structure Determination and Refinement

The position of the ANK domain was established by molecular replacement using PHASER (McCoy et al., 2007). Subsequently, the CTD, NTD, and BTD domains of CSL were placed through independent molecular replacement searches, followed by placement of MAML1 and DNA. The LLG score for the sequential molecular replacement runs were 71.9, 536.9, 1334.5, 1883.7, 2411.4, and 3184.6, respectively. The calculated RMSD for Cα atoms in the model after placing all the domains when compared to the previously reported structure without RAM (PDB code 2F8X) is 0.12 Å. The resulting phase was used to calculate difference maps (Figure S1), and the RAM polypeptide was modeled into the positive density using the *C. elegans* structure (PDB code 2FO1) as a guide for register. Refinement was carried out using DEN (Schröder et al., 2007, 2010), and a grid search was performed to optimize the DEN parameters using the SBGrid Science Portal for DEN (O'Donovan et al., 2012). Final refinement statistics are provided in Table S1. The test sets for calculating R_{free} are consistent between the current reported structure

and the previous structure without RAM (2F8X). Coordinates have been deposited with the PDB under accession number 3V79.

Hydrogen Exchange-Mass Spectrometry
Exchange Reactions

Stock protein solutions were prepared at 40 μM concentration or greater in buffer A. Deuterium labeling was initiated with a 15-fold dilution of the protein or complex sample (200 pmol for global exchange and 40 pmol for exchange studies utilizing pepsin digestion for fine mapping) into a D_2O buffer (99.96% D) containing 20 mM Tris, pD 8.1, 150 mM NaCl, and 5 mM DTT. At specific time points (10 s, 1 min, 10 min, 60 min, and 270 min) the labeling reaction was quenched by addition of an equal volume of ice cold quench buffer (100 mM potassium phosphate, pH 2.66) for global exchange analysis or ice cold denaturing quench buffer (0.8 M guanidinium chloride, 0.8% formic acid, pH 2) for pepsin digestion and subsequent local exchange analysis.

Global-Exchange Mass Analysis

Quenched protein samples were immediately injected onto a POROS 20 R2 protein trap and desalted with 0.05% trifluoroacetic acid (TFA) in water at a flow rate of 500 μl/min. The proteins were eluted into the mass spectrometer using a 15%–75% linear gradient of acetonitrile over 4 min at 50 μl/min with a Shimadzu HPLC system (LC-20AD). Mass spectral analyses were carried out with a Waters LCT-Premier[XE] mass spectrometer with a standard electrospray source, a capillary voltage of 3.2 kV, and a cone voltage of 35 V. Relative deuterium levels for each protein were calculated by subtracting the average mass of the undeuterated control sample from that of the deuterium-labeled sample. The deuterium levels were not corrected for back-exchange (Wales and Engen, 2006; Zhang and Smith, 1993).

Local-Exchange Mass Analysis

Immediately following the quench reaction, samples were treated with porcine pepsin in a 1:1 ratio of protein:enzyme and enzymatic digestion was allowed to proceed for 5 min on ice. Immediately following digestion, samples were injected into a Waters nanoACQUITY system with HDX technology for UPLC separation of peptic peptides (Wales et al., 2008). Separation was achieved after the peptides were trapped and desalted on a VanGuard Pre-Column trap (2.1 × 5 mm, ACQUITY UPLC BEH C18, 1.7 μm) for 3 min. Peptides were eluted from the trap using an 8%–40% linear gradient of acetonitrile over 12 min at a flow rate of 40 μl/min and were separated using an ACQUITY UPLC BEH C18 1.7 μm 1.0 × 100 mm column. Peptides that were produced from the enzymatic cleavage of the unlabeled protein were identified from the triplicate analysis of undeuterated control samples using a combination of Waters MS[E] technology on a Waters QTof Premier instrument and ProteinLynx Global Server (PLGS) searches of a customized database. All mass spectra indicated that all peptic peptides underwent exchange with EX2 kinetics.

All mass spectra were acquired using a Waters QTof Premier mass spectrometer with a standard electrospray source, a capillary voltage of 3.5 kV, and a cone voltage of 35 V. Duplicate sets of data were collected on two or three different days (for a total of four to six independent replicates per sample). Common peptides could be identified for each component in a minimum of two replicates; the experiments with these common peptides were plotted in Figures 3, 5, 6, and S3A–SC. Continuous-lock mass correction was accomplished with infusion of a peptide standard every 30 s for a mass accuracy of 3–5 ppm. The error of determining the average deuterium incorporation for each peptide was at or below ±0.2 Da (Houde et al., 2011). All mass spectra were processed with custom software supplied from WATERS, combined with HX-Express (Weis et al., 2006). Relative deuterium levels for each peptide were calculated by subtracting the average mass of the undeuterated control sample from that of the deuterium-labeled sample for isotopic distributions corresponding to the +1, +2, or +3 charge state of each peptide. Peptide maps in supplementary figures were created using MSTools (Kavan and Man, 2011). The data were not corrected for back exchange and are therefore reported as relative (Wales and Engen, 2006).

SUPPLEMENTAL INFORMATION

Supplemental Information includes three tables and six figures and can be found online at doi:10.1016/j.str.2011.12.011.

REFERENCES

Agrawal, N., Frederick, M.J., Pickering, C.R., Bettegowda, C., Chang, K., Li, R.J., Fakhry, C., Xie, T.X., Zhang, J., Wang, J., et al. (2011). Exome sequencing of head and neck squamous cell carcinoma reveals inactivating mutations in NOTCH1. Science *333*, 1154–1157.

Arnett, K.L., Hass, M., McArthur, D.G., Ilagan, M.X., Aster, J.C., Kopan, R., and Blacklow, S.C. (2010). Structural and mechanistic insights into cooperative assembly of dimeric Notch transcription complexes. Nat. Struct. Mol. Biol. *17*, 1312–1317.

Artavanis-Tsakonas, S., Rand, M.D., and Lake, R.J. (1999). Notch signaling: cell fate control and signal integration in development. Science *284*, 770–776.

Barrick, D., and Kopan, R. (2006). The Notch transcription activation complex makes its move. Cell *124*, 883–885.

Bertagna, A., Toptygin, D., Brand, L., and Barrick, D. (2008). The effects of conformational heterogeneity on the binding of the Notch intracellular domain to effector proteins: a case of biologically tuned disorder. Biochem. Soc. Trans. *36*, 157–166.

Bradley, C.M., and Barrick, D. (2006). The notch ankyrin domain folds via a discrete, centralized pathway. Structure *14*, 1303–1312.

Bray, S.J. (2006). Notch signalling: a simple pathway becomes complex. Nat. Rev. Mol. Cell Biol. *7*, 678–689.

Brou, C., Logeat, F., Gupta, N., Bessia, C., LeBail, O., Doedens, J.R., Cumano, A., Roux, P., Black, R.A., and Israël, A. (2000). A novel proteolytic cleavage involved in Notch signaling: the role of the disintegrin-metalloprotease TACE. Mol. Cell *5*, 207–216.

Del Bianco, C., Aster, J.C., and Blacklow, S.C. (2008). Mutational and energetic studies of Notch 1 transcription complexes. J. Mol. Biol. *376*, 131–140.

Englander, S.W., and Mayne, L. (1992). Protein folding studied using hydrogen-exchange labeling and two-dimensional NMR. Annu. Rev. Biophys. Biomol. Struct. *21*, 243–265.

Friedmann, D.R., Wilson, J.J., and Kovall, R.A. (2008). RAM-induced allostery facilitates assembly of a notch pathway active transcription complex. J. Biol. Chem. *283*, 14781–14791.

Fryer, C.J., Lamar, E., Turbachova, I., Kintner, C., and Jones, K.A. (2002). Mastermind mediates chromatin-specific transcription and turnover of the Notch enhancer complex. Genes Dev. *16*, 1397–1411.

Fryer, C.J., White, J.B., and Jones, K.A. (2004). Mastermind recruits CycC:CDK8 to phosphorylate the Notch ICD and coordinate activation with turnover. Mol. Cell *16*, 509–520.

Houde, D., Berkowitz, S.A., and Engen, J.R. (2011). The utility of hydrogen/deuterium exchange mass spectrometry in biopharmaceutical comparability studies. J. Pharm. Sci. *100*, 2071–2086.

Hvidt, A., and Linderstrøm-Lang, K. (1954). Exchange of hydrogen atoms in insulin with deuterium atoms in aqueous solutions. Biochim. Biophys. Acta *14*, 574–575.

Johnson, R.S., and Walsh, K.A. (1994). Mass spectrometric measurement of protein amide hydrogen exchange rates of apo- and holo-myoglobin. Protein Sci. *3*, 2411–2418.

Johnson, S.E., Ilagan, M.X., Kopan, R., and Barrick, D. (2010). Thermodynamic analysis of the CSL x Notch interaction: distribution of binding energy of the Notch RAM region to the CSL beta-trefoil domain and the mode of competition with the viral transactivator EBNA2. J. Biol. Chem. *285*, 6681–6692.

Katta, V., and Chait, B.T. (1991). Conformational changes in proteins probed by hydrogen-exchange electrospray-ionization mass spectrometry. Rapid Commun. Mass Spectrom. *5*, 214–217.

Kavan, D., and Man, P. (2011). MSTools—Web based application for visualization and presentation of HXMS data. Int. J. Mass Spectrom. *302*, 53–58.

Klinakis, A., Lobry, C., Abdel-Wahab, O., Oh, P., Haeno, H., Buonamici, S., van De Walle, I., Cathelin, S., Trimarchi, T., Araldi, E., et al. (2011). A novel tumour-suppressor function for the Notch pathway in myeloid leukaemia. Nature *473*, 230–233.

Kopan, R., and Ilagan, M.X. (2009). The canonical Notch signaling pathway: unfolding the activation mechanism. Cell *137*, 216–233.

Kovall, R.A., and Hendrickson, W.A. (2004). Crystal structure of the nuclear effector of Notch signaling, CSL, bound to DNA. EMBO J. *23*, 3441–3451.

Kovall, R.A., and Blacklow, S.C. (2010). Mechanistic insights into Notch receptor signaling from structural and biochemical studies. Curr. Top. Dev. Biol. *92*, 31–71.

Lubman, O.Y., Kopan, R., Waksman, G., and Korolev, S. (2005). The crystal structure of a partial mouse Notch-1 ankyrin domain: repeats 4 through 7 preserve an ankyrin fold. Protein Sci. *14*, 1274–1281.

Lubman, O.Y., Ilagan, M.X., Kopan, R., and Barrick, D. (2007). Quantitative dissection of the Notch:CSL interaction: insights into the Notch-mediated transcriptional switch. J. Mol. Biol. *365*, 577–589.

McCoy, A.J., Grosse-Kunstleve, R.W., Adams, P.D., Winn, M.D., Storoni, L.C., and Read, R.J. (2007). Phaser crystallographic software. J. Appl. Cryst. *40*, 658–674.

Mello, C.C., and Barrick, D. (2004). An experimentally determined protein folding energy landscape. Proc. Natl. Acad. Sci. USA *101*, 14102–14107.

Mumm, J.S., Schroeter, E.H., Saxena, M.T., Griesemer, A., Tian, X., Pan, D.J., Ray, W.J., and Kopan, R. (2000). A ligand-induced extracellular cleavage regulates gamma-secretase-like proteolytic activation of Notch1. Mol. Cell *5*, 197–206.

Nam, Y., Sliz, P., Pear, W.S., Aster, J.C., and Blacklow, S.C. (2007). Cooperative assembly of higher-order Notch complexes functions as a switch to induce transcription. Proc. Natl. Acad. Sci. USA *104*, 2103–2108.

Nam, Y., Sliz, P., Song, L., Aster, J.C., and Blacklow, S.C. (2006). Structural basis for cooperativity in recruitment of MAML coactivators to Notch transcription complexes. Cell *124*, 973–983.

Nam, Y., Weng, A.P., Aster, J.C., and Blacklow, S.C. (2003). Structural requirements for assembly of the CSL.intracellular Notch1.Mastermind-like 1 transcriptional activation complex. J. Biol. Chem. *278*, 21232–21239.

O'Donovan, D.J., Stokes-Rees, I., Nam, Y., Blacklow, S.C., Schröder, G.F., Brunger, A.T., and Sliz, P. (2012). A grid-enabled web service for low-resolution crystal structure refinement. Acta Crystallographica Section D., in press.

Otwinowski, Z., and Minor, W. (1997). Processing of X-ray diffraction data collected in oscillation mode. Methods Enzymol. *276*, 307–326.

Puente, X.S., Pinyol, M., Quesada, V., Conde, L., Ordóñez, G.R., Villamor, N., Escaramis, G., Jares, P., Beà, S., González-Díaz, M., et al. (2011). Whole-genome sequencing identifies recurrent mutations in chronic lymphocytic leukaemia. Nature *475*, 101–105.

Schröder, G.F., Brunger, A.T., and Levitt, M. (2007). Combining efficient conformational sampling with a deformable elastic network model facilitates structure refinement at low resolution. Structure *15*, 1630–1641.

Schröder, G.F., Levitt, M., and Brunger, A.T. (2010). Super-resolution biomolecular crystallography with low-resolution data. Nature *464*, 1218–1222.

Stransky, N., Egloff, A.M., Tward, A.D., Kostic, A.D., Cibulskis, K., Sivachenko, A., Kryukov, G.V., Lawrence, M.S., Sougnez, C., McKenna, A., et al. (2011). The mutational landscape of head and neck squamous cell carcinoma. Science *333*, 1157–1160.

VanderWielen, B.D., Yuan, Z., Friedmann, D.R., and Kovall, R.A. (2011). Transcriptional repression in the Notch pathway: thermodynamic characterization of CSL-MINT (Msx2-interacting nuclear target protein) complexes. J. Biol. Chem. *286*, 14892–14902.

Wales, T.E., and Engen, J.R. (2006). Hydrogen exchange mass spectrometry for the analysis of protein dynamics. Mass Spectrom. Rev. *25*, 158–170.

Wales, T.E., Fadgen, K.E., Gerhardt, G.C., and Engen, J.R. (2008). High-speed and high-resolution UPLC separation at zero degrees Celsius. Anal. Chem. *80*, 6815–6820.

Wallberg, A.E., Pedersen, K., Lendahl, U., and Roeder, R.G. (2002). p300 and PCAF act cooperatively to mediate transcriptional activation from chromatin templates by notch intracellular domains in vitro. Mol. Cell. Biol. *22*, 7812–7819.

Weis, D.D., Engen, J.R., and Kass, I.J. (2006). Semi-automated data processing of hydrogen exchange mass spectra using HX-Express. J. Am. Soc. Mass Spectrom. *17*, 1700–1703.

Weng, A.P., Nam, Y., Wolfe, M.S., Pear, W.S., Griffin, J.D., Blacklow, S.C., and Aster, J.C. (2003). Growth suppression of pre-T acute lymphoblastic leukemia cells by inhibition of notch signaling. Mol. Cell. Biol. *23*, 655–664.

Weng, A.P., Ferrando, A.A., Lee, W., Morris, J.P., 4th, Silverman, L.B., Sanchez-Irizarry, C., Blacklow, S.C., Look, A.T., and Aster, J.C. (2004). Activating mutations of NOTCH1 in human T cell acute lymphoblastic leukemia. Science *306*, 269–271.

Wilson, J.J., and Kovall, R.A. (2006). Crystal structure of the CSL-Notch-Mastermind ternary complex bound to DNA. Cell *124*, 985–996.

Zhang, Z., and Smith, D.L. (1993). Determination of amide hydrogen exchange by mass spectrometry: a new tool for protein structure elucidation. Protein Sci. *2*, 522–531.